NASA/TM—2008-215211 Paper no. 3114

A Cryogenic High-Power-Density Bearingless Motor for Future Electric Propulsion

Benjamin Choi
Glenn Research Center, Cleveland, Ohio

Mark Siebert
University of Toledo, Toledo, Ohio

June 2008

NASA STI Program . . . in Profile

Since its founding, NASA has been dedicated to the advancement of aeronautics and space science. The NASA Scientific and Technical Information (STI) program plays a key part in helping NASA maintain this important role.

The NASA STI Program operates under the auspices of the Agency Chief Information Officer. It collects, organizes, provides for archiving, and disseminates NASA's STI. The NASA STI program provides access to the NASA Aeronautics and Space Database and its public interface, the NASA Technical Reports Server, thus providing one of the largest collections of aeronautical and space science STI in the world. Results are published in both non-NASA channels and by NASA in the NASA STI Report Series, which includes the following report types:

- TECHNICAL PUBLICATION. Reports of completed research or a major significant phase of research that present the results of NASA programs and include extensive data or theoretical analysis. Includes compilations of significant scientific and technical data and information deemed to be of continuing reference value. NASA counterpart of peer-reviewed formal professional papers but has less stringent limitations on manuscript length and extent of graphic presentations.

- TECHNICAL MEMORANDUM. Scientific and technical findings that are preliminary or of specialized interest, e.g., quick release reports, working papers, and bibliographies that contain minimal annotation. Does not contain extensive analysis.

- CONTRACTOR REPORT. Scientific and technical findings by NASA-sponsored contractors and grantees.

- CONFERENCE PUBLICATION. Collected papers from scientific and technical conferences, symposia, seminars, or other meetings sponsored or cosponsored by NASA.

- SPECIAL PUBLICATION. Scientific, technical, or historical information from NASA programs, projects, and missions, often concerned with subjects having substantial public interest.

- TECHNICAL TRANSLATION. English-language translations of foreign scientific and technical material pertinent to NASA's mission.

Specialized services also include creating custom thesauri, building customized databases, organizing and publishing research results.

For more information about the NASA STI program, see the following:

- Access the NASA STI program home page at *http://www.sti.nasa.gov*

- E-mail your question via the Internet to *help@sti.nasa.gov*

- Fax your question to the NASA STI Help Desk at 301–621–0134

- Telephone the NASA STI Help Desk at 301–621–0390

- Write to:
  NASA Center for AeroSpace Information (CASI)
  7115 Standard Drive
  Hanover, MD 21076–1320

NASA/TM—2008-215211 Paper no. 3114

A Cryogenic High-Power-Density Bearingless Motor for Future Electric Propulsion

Benjamin Choi
Glenn Research Center, Cleveland, Ohio

Mark Siebert
University of Toledo, Toledo, Ohio

Prepared for the
2008 Propulsion-Safety and Affordable Readiness (P-SAR) Conference
cosponsored by the U.S. Army, Navy, and Air Force
Myrtle Beach, South Carolina, March 18–20, 2008

National Aeronautics and
Space Administration

Glenn Research Center
Cleveland, Ohio 44135

June 2008

Acknowledgments

Dr. Gerald Brown for his technical guidance throughout this work.

This work was sponsored by the Fundamental Aeronautics Program
at the NASA Glenn Research Center.

Level of Review: This material has been technically reviewed by technical management.

Available from

NASA Center for Aerospace Information
7115 Standard Drive
Hanover, MD 21076–1320

National Technical Information Service
5285 Port Royal Road
Springfield, VA 22161

Available electronically at http://gltrs.grc.nasa.gov

A Cryogenic High-Power-Density Bearingless Motor for Future Electric Propulsion

Benjamin Choi
National Aeronautics and Space Administration
Glenn Research Center
Cleveland, Ohio 44135

Mark Siebert
The University of Toledo
Toledo, Ohio 43606

Abstract

The NASA Glenn Research Center (GRC) is developing a high-power-density switched-reluctance cryogenic motor for all-electric and pollution-free flight. However, cryogenic operation at higher rotational speeds markedly shortens the life of mechanical rolling element bearings. Thus, to demonstrate the practical feasibility of using this motor for future flights, a non-contact rotor-bearing system is a crucial technology to circumvent poor bearing life that ordinarily accompanies cryogenic operation. In this paper, a bearingless motor control technology for a 12–8 (12 poles in the stator and 8 poles in the rotor) switched-reluctance motor operating in liquid nitrogen (boiling point, 77 K (–196 °C or –321 °F)) was presented. We pushed previous disciplinary limits of electromagnetic controller technique by extending the state-of-the-art bearingless motor operating at liquid nitrogen for high-specific-power applications. The motor was levitated even in its nonlinear region of magnetic saturation, which is believed to be a world first for the motor type. Also we used only motoring coils to generate motoring torque and levitation force, which is an important feature for developing a high specific power motor.

Objective

To develop self-levitation of a 12-8 switched-reluctance motor (SRM) operating into strong magnetic core saturation at liquid nitrogen temperature, where a super high-power-density motor operates.

Outline

I. Introduction
II. Motor Configuration
III. Review on Model-Based Controller Implementation
IV. A Proportional-Derivative (PD) Controller Implementation
V. Experimental Demonstration
VI. Experimental Characterization of Magnetic Bearing (M.B.) Force
VII. Summary

I. Introduction

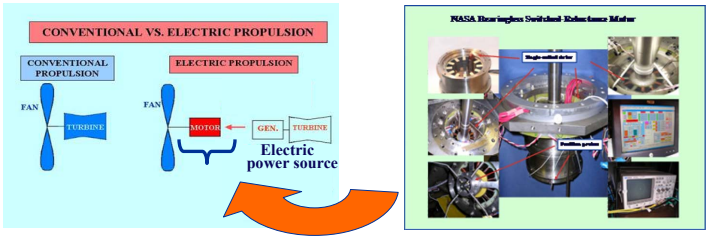

Figure 1. Electric propulsion system and NASA super high-power-density SRM.

- The NASA Glenn Research Center has been developing high-power-density motors for possible use for light weight and pollution-free flight. One suggested method of achieving that goal is a hydrogen-fueled aircraft that could use turbo-generators to develop electric power for motors that rotate the aircraft's propulsive fans or propellers.
- Adding extra subsystems to a turbine engine seems to make this concept impractical. However, overall system advantages of the electric propulsion compensates for the extra components, provided we achieve the power density required for an aircraft.

I. Introduction *(continued)*

Recently, we demonstrated improved performance of the NASA SRM, stemming mainly from LN_2 and LH_2 operation and coil design, surpassing (we believe) previous specific torque and specific tangential force records for the motor type. Furthermore, we anticipate more motor specific power by upgrading electric power conditioning and innovative coil windings.

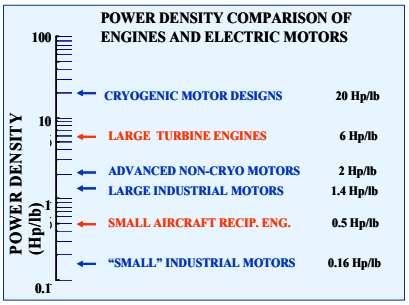

Figure 2. Power density comparison of engines and motors.

❖ A comparison of typical power densities in various motors and engines is shown. But notice that although cryogenic motors look better than turbine engines in this comparison, **turbine engines are prime movers**, developing shaft power from fuel, whereas motors are not prime movers.

❖ A complete comparison requires the additional weight of components that produce the electric power from fuel and any electric power conditioning electronics. A detailed description is in (G. Brown, 2005).

I. Introduction *(continued)*

- However, cryogenic operation at higher rotational speeds **markedly shortens** the life of mechanical rolling element bearings. Even without cryogenics, conventional bearing life may be limited at the high speeds possible with switched reluctance motors.
- Thus, to demonstrate the practical feasibility of using this high-power-density motor, a **non-contact rotor-bearing** system is a crucial technology.

Literature Survey of Bearingless Motors

- ✓ During the last decade, a variety of bearingless motors have been introduced, including permanent magnet, induction, and reluctance types. These motors have their own characteristics and applications.
- ✓ Among them, the **switched-reluctance motor** (SRM) is a favored candidate for the future airborne system because it has inherent fault-tolerance and rotor robustness and reliability at high rotational speeds (no coil windings on the rotor).
- ✓ In 2003, Takemoto developed a controllable radial bearing force equation for a 12-8 SRM at room temperature **by adding** a separate magnetic bearing coil winding to each stator pole motor winding for the rotor levitation – *making history* for a successful controller demonstration.

Our approach:

1. Extend self-levitation technique well into the strong magnetic core **saturated region** at LN_2 temperature, where GRC's Cryogenic High-Power-Density Motor operates.
2. No separate coils for motor action and magnetic bearing action, but **only motor coils** as in a conventional motor configuration. We favor the single-coil approach because it is more conducive to higher specific power.
3. A practical self-levitation technique using an observation-based PD control algorithm, which does **not require** any nonlinear mathematical **plant models** and is advantageous at high motor speed due to less computationally intensive method.
4. Experimental characterization of magnetic bearing force.

II. Motor Configuration

- The motor is mounted with a vertical axis to simplify submersion in LN_2.
- Axial length of the lamination stack is 1.97 in (5.08 cm).
- The radial air gap is 20 mils (0.051 cm). The stator-pole arc, the stator-pole-gap arc and the rotor-pole arc are all equal.
- The laminations are 6 mils (0.152 mm) thick and are made of Hiperco 50 HS.

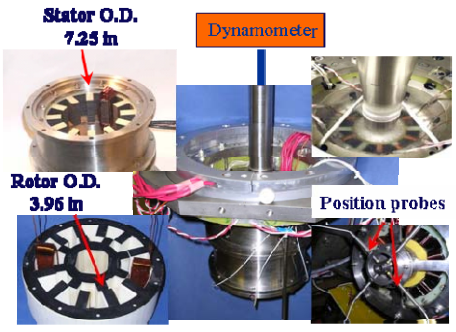

Figure 3. NASA bearingless switched reluctance motor.

When operated on conventional rolling element bearings

- ✓ Achieved the specific torque of 1.8 ft-lb/lb and specific power of 10.6 Hp/lb-EM.
- ✓ Anticipate more specific power by upgrading electric power conditioning and better coil windings.

II. Motor Configuration *(continued)*

- The arc angle of the rotor and stator teeth is 15º. The motor winding on each stator pole is connected to an independent power amplifier (±170 Vmax and ±15 A rms continuous current).
- Since there are no separate levitation coils, the required motoring and levitating currents for each pole are mathematically summed and applied as a **single current** to the motor pole winding.
- Square-wave excitation current is applied to energize each phase. The motoring torques and levitation forces are generated by these three phases (A, B, and C) for every 15º, between the start of overlap and aligned positions.

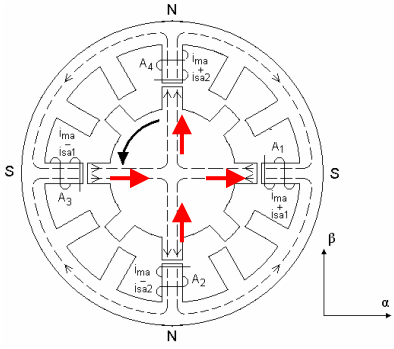

Figure 4. Phase A motor winding configuration and levitation currents polarity of the 12-8 SRM.

Principle of radial force generation

The motoring current generates a biasing flux in the α-direction. The flux density is increased at one air gap and decreased at the other air gap by the flux density generated by the 2-pole radial force current i_{a1}. **This superimposed imbalance** of flux density results in the radial force F_α acting on the rotor in the α-direction.

Similarly, a radial force in the β-direction can be produced. Thus, radial force can be generated in **any desired direction.**

III. Review on Model-Based Controller Implementation

Since a model-based controller will be compared with the proposed controller, a quick review of its controller implementation is given. The radial forces F_α and F_β can be derived as

Plugging our motor's configuration into radial force formula gives

$$F_\alpha = \frac{\partial W_a}{\partial \alpha} = N^2\left[\frac{\mu_o hr(\pi - 12\theta_a)}{6l_o^2} + \frac{32\mu_o hrc\theta_a}{\pi\left(4rc\theta_a(l_o+\alpha)+\pi l_o^2\right)}\right] i_{ma} i_{sa1}$$

$$F_\beta = \frac{\partial W_a}{\partial \beta} = N^2\left[\frac{\mu_o hr(\pi - 12\theta_a)}{6l_o^2} + \frac{32\mu_o hrc\theta_a}{\pi\left(4rc\theta_a(l_o+\beta)+\pi l_o^2\right)}\right] i_{ma} i_{sa2}$$

Stack length, h	**2 in**
Average air-gap length, l_g	**20 mils**
Constant, c	**1.49**
Rotor pole radius, r	**1.98 in**
Number of turns of main winding, N	**80**
Motoring current, i_m	**8 amps**
Levitation current in x-axis, i_{sa1}	**2 amps**
Levitation current in y-axis, i_{sa2}	**2 amps**

Table 1. A summary of main dimensions of the motor and parameters for the radial force calculation.

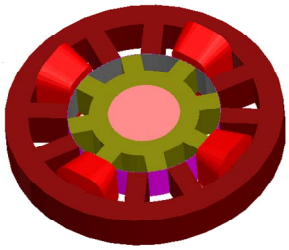

Figure 5. A Maxwell 3-D model of the motor for FEM analysis

Model-Based Controller Implementation *(continued)*

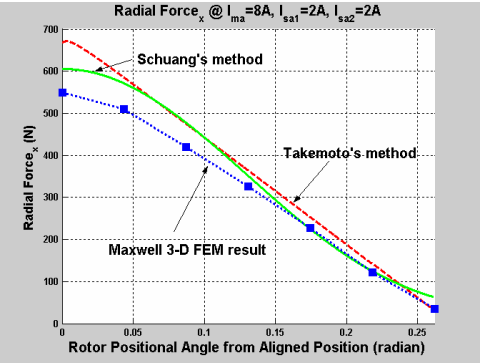

Figure 6. Static radial force prediction calculated by using Takemoto's formula, Shuang's new formula, and a Maxwell 3-D FEM analysis.

- Takemoto's force equation was selected to be implemented in the model-based controller because it is easier to invert for calculating the levitation control current.
- However, the **difference** between Takemoto's radial force prediction and the FEM result was utilized in our controller to minimize the required control current error.

➔ For instantaneous rotor angle for each phase, the levitating current is **increased by the ratio** of Takemoto's force to the FEM force from 0º to 15º (0.262 radians) of the rotor positional angles.

IV. A PD (Proportional-Derivative) Controller Implementation

- In this section, we present an observation-based controller using a PD control scheme, which does **not require a plant model** for controller design.
- The only constraint is that the levitation current cannot be greater than the motoring current to **avoid the polarity change** of stator pole for each phase.

$$i(x,\dot{x}) = -\frac{(k+k_s)\cdot x + d\cdot \dot{x}}{k_i}$$

A proportional gain includes a term to offset the negative bearing stiffness and one to produce the actual bearing net stiffness. Derivative gain controls the damping of the rotor radial positions.

Establish stability map

- Determine which combinations of proportional and derivative gains produce stable operation.
- Beginning at a low speed, a stability map was obtained experimentally at each successive speed by changing one gain with the other gain fixed until the rotor orbit hits the predefined orbit limit.
- These gain sets show stability surface under which stable operation of the system is achieved at the entire operating range.
- While testing the new controller parameters, the middle range gain set is selected and plugged into the controller as a **safe gain** set.

A PD Controller Implementation *(continued)*

MatLab/Simulink software was used for a closed-loop simulation and a dSPACE system was used for the real-time motor control system.

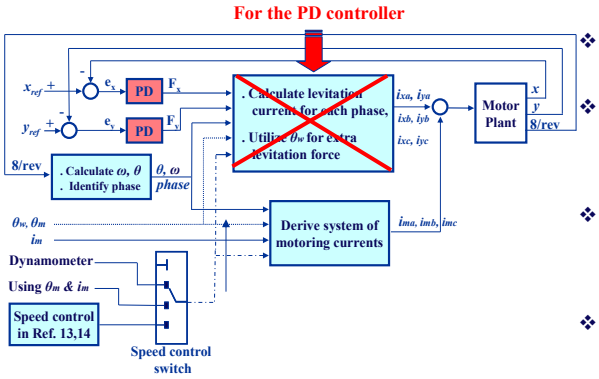

Figure 7. Simplified block diagram of control system.

- Auto kick-start at the beginning of motor operation.
- An eight/rev signal is fed back to calculate the rotor angular position and speed and to identify the phase.
- Four position probes sense the shaft radial position and those signals are fed back for magnetic bearing action.
- For the Phases B and C, a transformation matrix is used.
- Software speed control switch to select one of three choices for the motor speed control.

A PD Controller Implementation *(continued)*

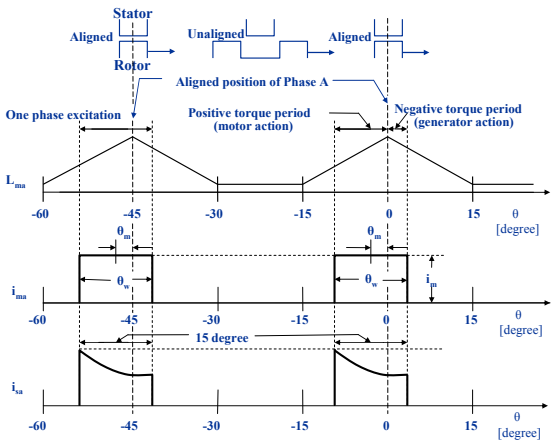

Figure 8. Phase A energizing for motoring and levitation.

Speed Control Option

- The first option is a dynamometer that is attached to the top of the motor, which controls the motor up to 20,000 rpm.
- The second is an open-loop control in which we choose the firing angle, pulse width and the motoring current to manipulate the amount of positive and negative torques.
- The last option is a closed-loop speed control (proposed by Takemoto et al.) which has been successfully implemented.

A PD Controller Implementation *(continued)*

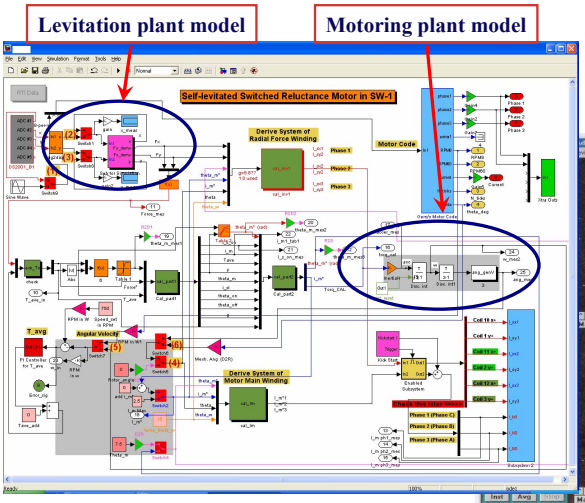

Figure 9. Matlab/Simulink closed-loop system model that represents the bearingless motor control system.

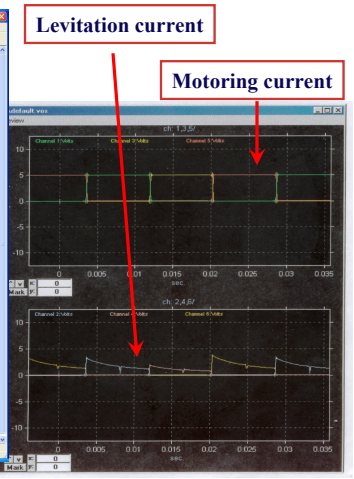

Figure 10. Closed-loop simulation result.

A PD Controller Implementation *(continued)*

This control cockpit window allows …

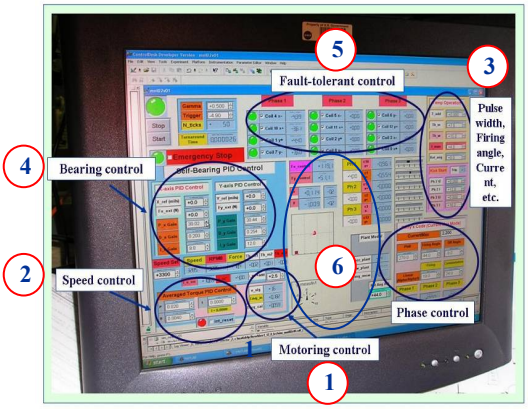

Figure 11. A user-friendly controller cockpit window for the dSPACE control system.

1) Modification of motoring control parameters.
2) Speed control method,
3) Pulse width, firing angle, auto kick-start.
4) Stiffness and damping gains for the PD controller.
5) Fault-tolerance.
6) In addition, a simple data acquisition capability for the rotor orbit and control command signals for each phase is added to monitor the system performance.

V. Experimental Demonstration

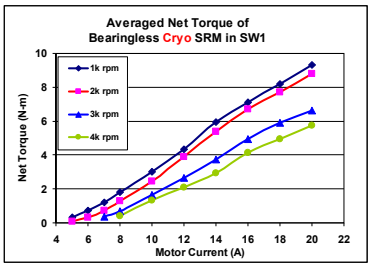

Fig. 12: Averaged net torque of bearingless cyro SRM.

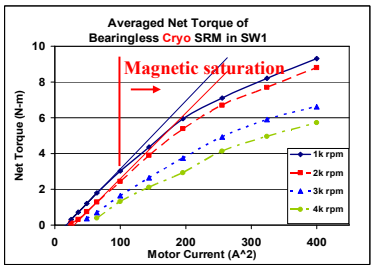

Fig. 13: Averaged net torque of bearingless cyro SRM vs. A^2.

- Measured averaged net torque of the bearingless cryo SRM using dynamometer changing motoring current I_b from 5 A to 20 A.
- Fig. 13 shows the relation of torque and current squared to see where magnetic core saturation occurred. The saturation occurred after 10A.
- Thus, Fig. 12 shows the self-levitation operating from linear region **into strong magnetic core saturation** at LN_2 temperature..
- Here, the maximum control current for the rotor levitation was set to 10% of motoring I_b, and the combined current level cannot exceed 22 A for our power amplifier safety.

V. Experimental Demonstration *(continued)*

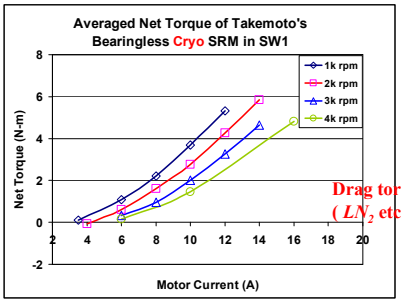

Fig. 14: Averaged net torque of modified Takemoto's bearingless cyro SRM.

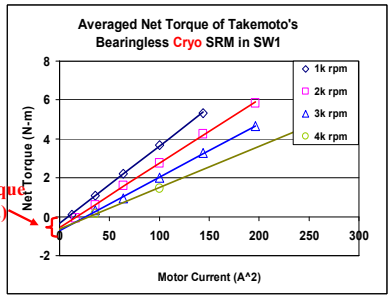

Fig. 15: Averaged net torque of modified Takemoto's bearingless cyro SRM vs. A^2.

- The modified Takemoto's linear controller was tested and the experimental averaged net torque was obtained changing I_B from 4 A to 16 A as shown in Fig. 14.
- Fig. 15 shows that the relation of torque and current squared is still linear. Obtained experimental **drag torque** of 0.33 N-m at 1k rpm; 0.52 N-m at 2k rpm; 0.70 N-m at 3k rpm; 0.65 (?) N-m at 4k rpm.
- This linear-model-based controller worked up to 14 A, including nonlinear region between 10 A and 14 A.

V. Experimental Demonstration *(continued)*

Rotor orbits at 1k rpm

- The rotor orbits at 1k rpm changing I_B from 4 A to 22 A.
- The rotor orbits were relatively small and solid over the linear and nonlinear regions.
- Notice that even the largest rotor orbits are within **12%** of backup bearing clearance and the required levitation current is less than **10%** of the motoring current.

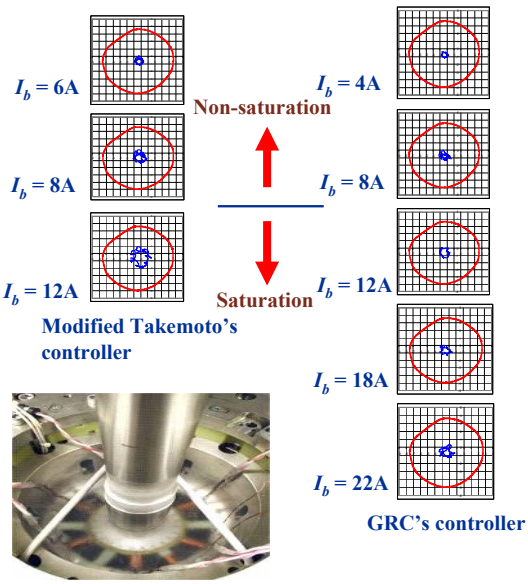

V. Experimental Demonstration *(continued)*

GRC controller

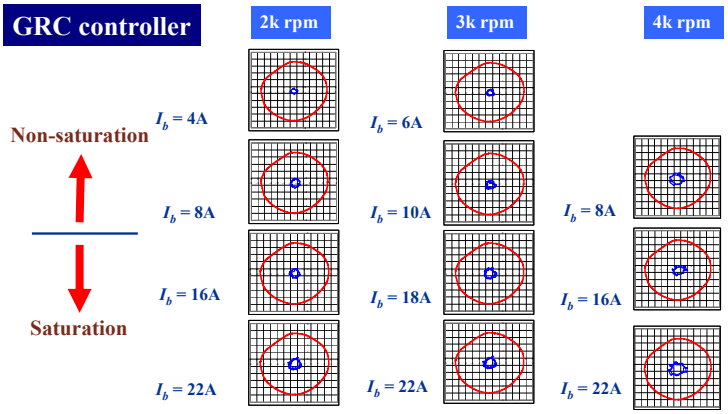

- This figure shows the rotor orbits from 2k rpm to 4k rpm, maximum allowable speed at that time, changing I_B from 4 A to 22 A.
- The rotor orbits were still relatively small and solid over the linear and nonlinear regions.

Command and current signals at 4k rpm

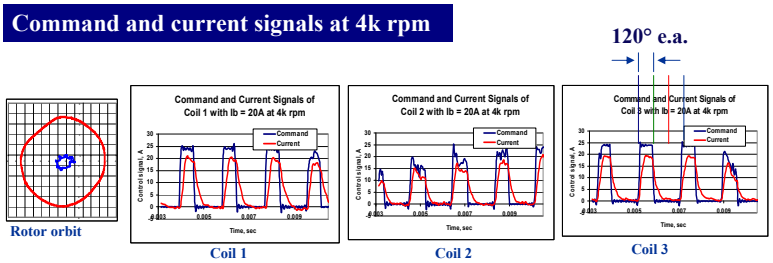

- This figure shows rotor orbit within backup bearing clearance circle, command signal from the controller and actual current applied to power amplifier for each phase at 4k rpm.
- For high speed, the actual current signals could not follow the command signals and started dropping even before reaching the command level.
- In our work, we selected 120° (electrical angle) pulse width θ_w to demonstrate the worst scenario – **no overlap** between adjacent phases.

V. Experimental Demonstration *(continued)*

Exp. torque comparison with full motoring case (no rotor levitation)

SW-1 Cryo SRM Torque at High Current – Exp. and Cal. (G. Brown, 2003)

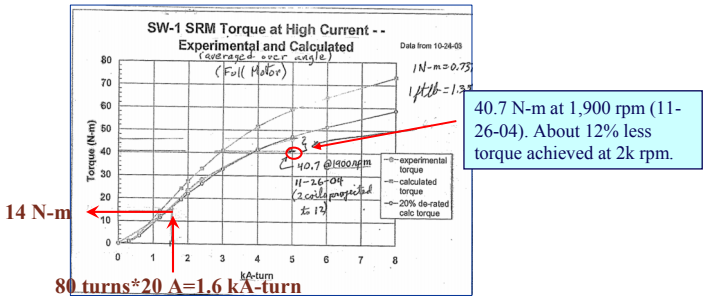

40.7 N-m at 1,900 rpm (11-26-04). About 12% less torque achieved at 2k rpm.

- From the chart, the full motoring torque at 2k rpm with I_B=*20 A* can be obtained as about 12.4 N-m (88% of 14 N-m), while the bearingless motoring torque at the same condition is about 8.8 N-m. ➔ About **28% loss**.
- This loss came mainly from the **rotor levitation** and **pulse width** (120° electrical angle for the self-levitation motor and 180° for full motoring case).
- If pulse width θ_w is 180°, we would drastically reduce the loss.

VI. Experimental Characterization of Magnetic Bearing (MB)

Linearized magnetic bearing force is

$$F = -Kx - gI_C = (K_B - K_f)x - gI_C$$

where K_B: negative stiffness, K_f: bearing net stiffness, g: current stiffness.

1. Experimental negative stiffness

1) Set the control current I_C to zero. Locate the rotor at fully aligned position and activate coils 3 and 6 (half phase 3) using I_B.
2) Two rails mounted to block y-directional displacement.
3) Starting from wall, move the rotor to magnetic center using a pusher with load cell housing.
4) Measure several displacement-force curves by varying I_B value and then normalize them by I_B.

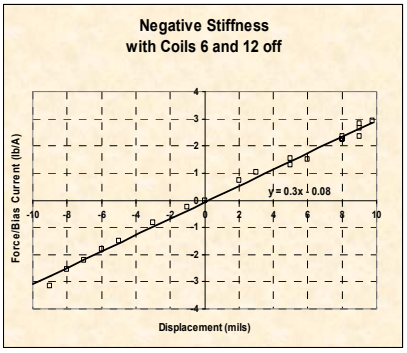

➔ We applied I_B from 3A to 7A and obtained negative stiffness per I_B as (3 lb*6)/10 mils = **800 lb/A-in**. In reality, data near origin are S-shaped, but we had difficulty getting data there and thus it is linearized for simplicity.

2. Experimental current stiffness

1) Due to difficulty resulting from *IB*=0, we had to set the control current I_C as well as bias current.
2) Push the load cell until it hits the wall.
3) Measure several control current-force curves by varying I_B value and then normalize them by I_B.

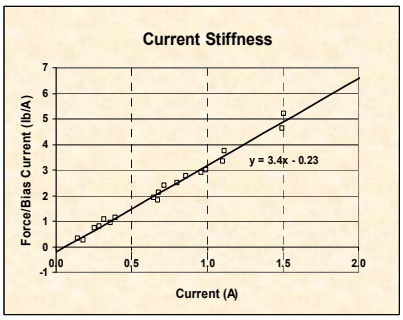

- The current stiffness per motoring current I_B, over the range from 3 A to 7 A, was obtained as (3.4 lb*6)/A^2 = **20.4 lb/A^2**.
- Only the room temperature case was measured because LN_2 dewar blocked the displacement gauge at that time.

VII. Summary

- Successfully demonstrated the NASA self-levitated high-power-density SRM using **only motoring coils** (no separate levitation coils) – an important feature for developing a high specific power motor.
- Extended the self-levitation well into the strong magnetic core **saturated region** at LN_2 temperature, where a super high-power-density motor operates.
- Experimental averaged net torque and **characterization** of magnetic bearing force were obtained.
- Our observation-based controller did **not require a non-linear plant model** and reduced actual loop-time by **67%** (45 μs ➔ 15 μs) compared with Takemoto's linear controller (nonlinear controller would be even slower) – faster real-time calculation at much higher rotor speed.

REPORT DOCUMENTATION PAGE	Form Approved OMB No. 0704-0188

1. REPORT DATE *(DD-MM-YYYY)*	2. REPORT TYPE	3. DATES COVERED *(From - To)*
01-06-2008	Technical Memorandum	

4. TITLE AND SUBTITLE
A Cryogenic High-Power-Density Bearingless Motor for Future Electric Propulsion

5a. CONTRACT NUMBER

5b. GRANT NUMBER

5c. PROGRAM ELEMENT NUMBER

6. AUTHOR(S)
Choi, Benjamin; Siebert, Mark

5d. PROJECT NUMBER

5e. TASK NUMBER

5f. WORK UNIT NUMBER
WBS 561581.02.08.03.15.03

7. PERFORMING ORGANIZATION NAME(S) AND ADDRESS(ES)
National Aeronautics and Space Administration
John H. Glenn Research Center at Lewis Field
Cleveland, Ohio 44135-3191

8. PERFORMING ORGANIZATION REPORT NUMBER
E-16485

9. SPONSORING/MONITORING AGENCY NAME(S) AND ADDRESS(ES)
National Aeronautics and Space Administration
Washington, DC 20546-0001

10. SPONSORING/MONITORS ACRONYM(S)
NASA

11. SPONSORING/MONITORING REPORT NUMBER
NASA/TM-2008-215211

12. DISTRIBUTION/AVAILABILITY STATEMENT
Unclassified-Unlimited
Subject Category: 07
Available electronically at http://gltrs.grc.nasa.gov
This publication is available from the NASA Center for AeroSpace Information, 301-621-0390

13. SUPPLEMENTARY NOTES

14. ABSTRACT
The NASA Glenn Research Center (GRC) is developing a high-power-density switched-reluctance cryogenic motor for all-electric and pollution-free flight. However, cryogenic operation at higher rotational speeds markedly shortens the life of mechanical rolling element bearings. Thus, to demonstrate the practical feasibility of using this motor for future flights, a non-contact rotor-bearing system is a crucial technology to circumvent poor bearing life that ordinarily accompanies cryogenic operation. In this paper, a bearingless motor control technology for a 12-8 (12 poles in the stator and 8 poles in the rotor) switched-reluctance motor operating in liquid nitrogen (boiling point, 77 K (-196 °C or -321 °F)) was presented. We pushed previous disciplinary limits of electromagnetic controller technique by extending the state-of-the-art bearingless motor operating at liquid nitrogen for high-specific-power applications. The motor was levitated even in its nonlinear region of magnetic saturation, which is believed to be a world first for the motor type. Also we used only motoring coils to generate motoring torque and levitation force, which is an important feature for developing a high specific power motor.

15. SUBJECT TERMS
Self-levitation; Magnetic bearings; Cryogenics; Magnetic suspension; Switched-reluctance motor; Magnetic saturation; High-power-density motor

16. SECURITY CLASSIFICATION OF:			17. LIMITATION OF ABSTRACT	18. NUMBER OF PAGES	19a. NAME OF RESPONSIBLE PERSON
a. REPORT	b. ABSTRACT	c. THIS PAGE			STI Help Desk (email:help@sti.nasa.gov)
U	U	U	UU	19	19b. TELEPHONE NUMBER *(include area code)* 301-621-0390